Luke C. Olson[1]
Savannah River National Laboratory, SRNL, Aiken SC, 29808
e-mail: luke.olson@srnl.doe.gov

Roderick E. Fuentes
Savannah River National Laboratory, SRNL, Aiken SC, 29808

Michael J. Martinez-Rodriguez
Savannah River National Laboratory, SRNL, Aiken SC, 29808

James W. Ambrosek
Woodward Inc., 1000 East Drake Road, Fort Collins, CO 80525

Kumar Sridharan
Department of Engineering Physics, University of Wisconsin-Madison, 1500 Engineering Drive, Madison WI, 53711

Mark H. Anderson
Department of Engineering Physics, University of Wisconsin-Madison, 1500 Engineering Drive, Madison WI, 53711

Brenda L. Garcia-Diaz
Savannah River National Laboratory, SRNL, Aiken SC, 29808

Joshua Gray
Savannah River National Laboratory, SRNL, Aiken SC, 29808

Todd R. Allen
Department of Engineering Physics, University of Wisconsin-Madison, 1500 Engineering Drive, Madison WI, 53711

Impact of Corrosion Test Container Material in Molten Fluorides

The effects of crucible material choice on alloy corrosion rates in immersion tests in molten LiF–NaF–KF (46.5–11.5-42 mol. %) salt held at 850 °C for 500 hrs are described. Four crucible materials were studied. Molten salt exposures of Incoloy-800H in graphite, Ni, Incoloy-800H, and pyrolytic boron nitride (PyBN) crucibles all led to weight-loss in the Incoloy-800H coupons. Alloy weight loss was ~30 times higher in the graphite and Ni crucibles in comparison to the Incoloy-800H and PyBN crucibles. It is hypothesized galvanic coupling between the alloy coupons and crucible materials contributed to the higher corrosion rates. Alloy salt immersion in graphite and Ni crucibles had similar weight-loss hypothesized to occur due to the rate limiting out diffusion of Cr in the alloys to the surface where it reacts with and dissolves into the molten salt, followed by the reduction of Cr from solution at the molten salt and graphite/Ni interfaces. Both the graphite and the Ni crucibles provided sinks for the Cr, in the formation of a Ni–Cr alloy in the case of the Ni crucible, and Cr carbide in the case of the graphite crucible.
[DOI: 10.1115/1.4031682]

Introduction

Molten fluoride systems using both Cr bearing alloys and graphite or Ni may be at heightened risk for Cr dealloying. Examples include proposed concentrated solar power (CSP) applications, heat treatment baths, advanced high temperature nuclear reactors, heat transport loops, and general materials research. Molten salt CSP applications have attracted interest from the DOE-EERE (U.S. Department of Energy Office of Energy Efficiency and Renewable Energy) funded SunShot initiative. Benefits for CSP includes use for thermal energy storage [1] and raising heat-to-electricity conversion efficiencies of solar power towers to about 50% [2]. Molten salt-fueled reactors and molten salt cooled reactors such as the AHTR (advanced high temperature reactor) may also encounter this interaction. Graphite is often present in the core or as fuel compacts for these reactor designs. Ni plated/welded surfaces have been proposed in these concepts and could cause similar reactions [3,4]. Interactions between materials exposed to a molten salt medium complicate the use of heat transfer loops. Heat transfer loops often rely on multiple

[1]Corresponding author.
Contributed by the Solar Energy Division of ASME for publication in the Journal of Solar Energy Engineering: Including Wind Energy and Building Energy Conservation. Manuscript received October 8, 2014; final manuscript received September 1, 2015; published online October 15, 2015. Assoc. Editor: Prof. Nathan Siegel.

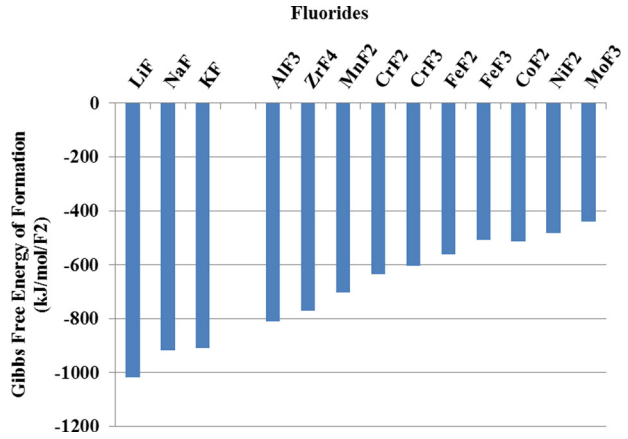

Fig. 1 Gibbs free energy of fluoride formation per F_2 molecule of metals present in the salt and materials at 850 °C. The more negative the Gibb's free energy of formation an alloy constituent is in comparison to the salt constituents, the less stable it will likely be in the molten salt.

alloys and may use alloy piping in combination with ceramic heat exchangers (possibly PyC or SiC coated composites). Such designs have been proposed to transport heat between a high temperature nuclear reactor and a chemical process or H_2 production plant [4]. It would be beneficial to determine impact of corrosion test container materials on experimental results to improve testing repeatability and to better compare results between researchers.

This paper details interactions between Cr bearing alloys and Ni, graphite, alloy, and ceramic crucibles. The discussion focuses on 850 °C 500 hrs immersion tests utilizing a fluoride based salt, FLiNaK. FLiNaK is a ternary eutectic alkali fluoride salt (LiF–NaF–KF: 46.5–11.5–42 mol. %) and was selected for the corrosion tests based on an analysis [5] that identified it as a candidate heat transfer fluid. The primary mechanism and driving forces for alloy corrosion in fluoride based salts are well understood and documented [1,5–8]. The Gibbs free energy of formation of metal fluorides formed by constituent elements of the alloys can be used to determine the most stable fluoride compounds likely to form in FLiNaK (Fig. 1). The elements with the most negative Gibbs free energies of formation are selectively attacked in an alloy by oxidative components in molten fluoride salts [5]. Oxidants in salts arise from impurities in salt constituents, such as oxides, contaminant chlorides less stable than the main salt constituents, moisture, and can be introduced during operation of molten salt systems. Once an oxidant has been introduced, cyclic corrosion

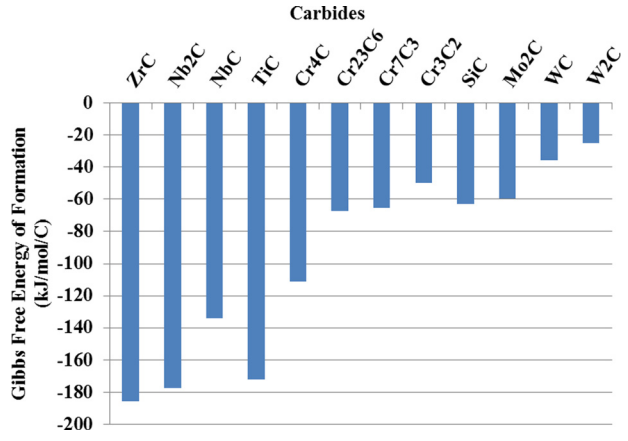

Fig. 2 Gibbs free energy of carbide formation per C atom for elements present in the alloys at 850 °C. Favorable reactions have more negative Gibb's free energy of formations.

mechanisms can then proceed. Likewise, the Gibbs free energy of formation of metal carbides (Fig. 2) formed from the alloying elemental constituents can determine the elements likely to form carbides.

Corrosion increases as Cr and C content increases for Fe-based and Ni-based alloys exposed to molten FLiNaK salt when a driving force for Cr dissolution is present [8]. Mass loss from a diverse number of alloys exposed to molten FLiNaK salt in graphite crucibles is summarized in depth elsewhere [7]. Although the mechanism of corrosion for Fe-based and Ni-based alloys is similar, molten salt exposures in different crucible materials and a variety of alloy coupons presents different weight-loss rates. For most of the high temperature alloys tested, Cr is the active primary metal component and selectively attacked by oxidants in the salt [5]. Cr also forms carbides that can concentrate in the grain boundary regions. Cr principally dealloys at the surface and grain boundaries that serve as accelerated pathways for Cr to reach the alloy/salt interface, and to a lesser extent through the bulk alloy crystals near the surface. The affected depth increases with time. Many of the fluorides in Fig. 1 are soluble in FLiNaK or have low melting points. For example, Cr fluorides have calculated equilibrium concentration of 2600 ppm at 800 °C in LiF–NaF–KF–UF_4 (41.0–11.2–45.3–2.5 mol. %) [9] and melts at 894 °C.

Several types of reactions can occur between materials in molten salts. In the Hall–Héroult Al extraction process, the molten salt mixture (primarily Na_3AlF_6 with dissolved Al_2O_3) forms graphite intercalation compounds and cyanide in the graphite pot liners [10]. One carburizing process [11] relies on a chloride salt mixture and graphite particles dispersed in the salt by mechanical agitation [11]. Graphite rods rectify chloride heat treatment baths by reducing metal oxide corrosion products to metals that adhere to the rods [12]. Similar alloy/graphite and alloy/alloy interactions in molten heat treatment salts have also been described where select elements are transported from one alloy to another material [13,14].

Experimental

Unless otherwise stated, FLiNaK salt was procured from Electrochemical Systems, Inc. (ECS), in Oak Ridge, TN, where the salt was made using high purity ingredients in a graphite crucible before being pumped into a Ni crucible for shipment. The ECS salt underwent a hydrofluorination process involving sparging with a H_2/HF gas mixture after fusion to remove oxide and moisture impurities. Two other salts were also used to determine the impact of the salt purification process in the immersion tests. A salt made by researchers at Idaho National Laboratory (INL) used similar high purity ingredients, but did not undergo chemical purification. The INL salt components were mixed in a glassy carbon crucible, and purged with argon gas while being heated in 100 °C steps until reaching 670 °C. University of Wisconsin (UW) researchers made another salt in a similar fashion to the INL procured salt. However, the UW salt fabrication process withdrew the argon purge tube at 400 °C.

The alloys were procured through commercial sources. Table 1 lists the compositions of the alloys, rounded to the nearest tenth of a percent. The alloys were selected for corrosion testing based on

Table 1 Compositions (wt.%) of the alloys discussed in the present study, rounded to nearest tenth of a percent and neglecting elements below a tenth of a percent

Alloy	Cr	Mo	W	Al	Ti	Fe	C	Co	Ni	Mn
Hastelloy-N	6.3	16.1	0.1			4.0	0.03	0.2	72.2	0.5
Incoloy-800H[a]	20.4			0.5	0.6	45.3	0.07		31.6	0.8
Ni-201						0.1	0.02		99.4	0.2

[a]Several similar Incoloy-800H heats were used.

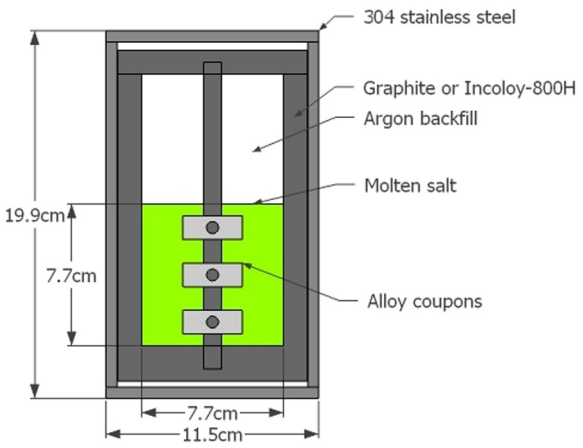

Fig. 3 Schematic illustration of one corrosion capsule apparatus used in the present study for testing corrosion performance of alloys in molten FLiNaK salt at 850 °C for 500 hrs. Dimensions are in centimeters. This design utilized graphite or Incoloy-800H for the crucible material.

their high temperature strength, code certification, and history of high temperature use.

Two designs were used for corrosion capsules for the immersion tests, each with two crucible materials. The corrosion capsule was welded shut in an argon atmosphere glove box for the first design. In this design, both high-density graphite and Incoloy-800H crucibles were separately used to contain the molten salt (Fig. 3). Further details of the design are discussed elsewhere [6,7]. Figure 4 shows a sketch of the second corrosion cell design. The second design separately used both Ni and PyBN crucibles. The corrosion cell was a modified induction heating vacuum melting vessel with a water cooled compression seal procured from MTI Corporation. For immersion tests, the corrosion cell was placed upright in a vertical tube furnace with the sealing flange outside of the heated zone. The first corrosion cell design had an area of graphite or Incoloy-800H crucible exposed to molten salt of ~260 cm^2, exposed alloy area of about 24 cm^2, with a volume of salt of about 360 cm^3. The second corrosion cell design had an exposed Ni or PyBN crucible area of about 90 cm^2, exposed alloy area of about 8 cm^2, and a volume of salt of about 110 cm^3. For both experimental designs, the ratio of salt exposed crucible to sample area was ~11.

In the first corrosion cell design graphite was chosen as a container material because it is not corroded by molten fluorides [15]. The graphite, grade AXZ-5Q1, was obtained from POCO Graphite, Inc, of Decatur, TX. The POCO graphite had an average particle size of 5 μm and a pore size of 0.7 μm [16]. Additionally, because purity of the salt was a concern, the graphite was purified (total ash range 5 ppm or less) [17]. Prior to sample introduction and cell assembly, the graphite crucible was heated up to 1000 °C for 10 hrs in an Ar atmosphere to remove residual moisture and oxygen. Some oxides may have remained in the graphite. The furnace argon cover gas contained less than <5 ppm H_2O, <5 ppm O_2, and less than 2 ppm hydrocarbons. After the graphite crucibles were cooled, they were removed from the argon furnace and immediately placed in an argon atmosphere glove box where the corrosion cells were assembled. The crucibles were exposed to air during the brief transport from the furnace to the antechamber. Mirror polished alloy coupons were then placed in the corrosion cells. The alloy coupons did not receive any treatment aside from the mirror polishing to remove most residual surface oxides and present a surface more easily characterized post corrosion. The graphite crucible was sealed in a 304 stainless steel (SS) capsule prior to corrosion testing. Residual oxides in the graphite and on the polished metal coupons, and oxygen and moisture on the surfaces of the graphite from air exposure during transport from the furnace to the glove box antechamber, could have impacted test results. Incoloy-800H corrosion capsules, similar to the graphite capsules shown in Fig. 3, where the graphite components were made out of Incoloy-800H, were also used for corrosion tests that used Incoloy-800H coupons. Ni and PyBN crucibles were not used in the first corrosion cell design. Ni and PyBN crucibles were used in the second corrosion cell design to determine acceleration in corrosion occurring because of the graphite, and how it varies for specific alloys. For the graphite and Incoloy-800H crucible corrosion tests, three coupons per crucible were exposed to FLiNaK, for the Ni and PyBN crucible corrosion tests one coupon per crucible was exposed and 1/3 of the salt was used. The salts were kept in an Ar environment, and welds for the SS air boundary crucible occurred inside of an Ar atmosphere glove box with <1 ppm O_2 and 2 ppm or less H_2O.

In the second corrosion, cell design coupons were hung from a Ni-201 cap using Ni wire or binderless, sintered BN (boron nitride) (Grade AX05, Saint-Gobain). The coupon would then be placed in a Ni or PyBN crucible with the cap resting on top of the crucible. The salt filled crucible was then placed in a SS envelop with some tantalum foil (to getter oxygen), and the SS envelop folded shut. The bagged SS crucibles were then placed up to two at a time in a large SS tube sealed on the bottom. More tantalum foil was placed underneath and on top of the bagged crucibles. Carbon foam was placed on top of the bagged crucibles. The carbon foam insulated the top sealing flange from heat while the part of the cell below the carbon foam was kept in a furnace. Near the base of each crucible, on the outside of the SS bags, thermocouple probes would be placed to monitor the temperature. The temperature difference was kept to below 10 °C. During testing, a constant

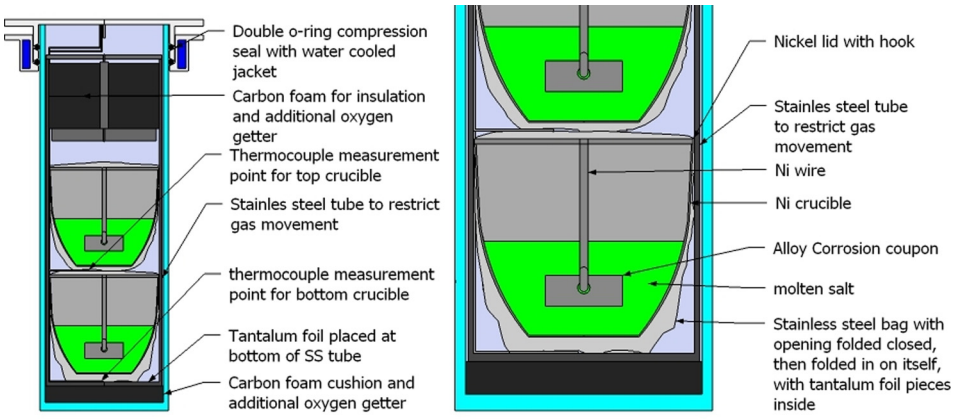

Fig. 4 Sketch of corrosion cells used in research

Table 2 Weight-loss measurements from 500 hrs, 850 °C, FLiNaK molten salt immersion tests. Scale accuracy and precision are believed to be dominant source of coupon weight change deviation for Ni-201 and Incoloy-800H in Incoloy-800H crucible.

Alloy	Graphite crucible weight-loss (mg/cm^2)	Ni crucible weight-loss (mg/cm^2)	PyBN crucible weight-loss (mg/cm^2)	800H crucible weight-loss (mg/cm^2)
Ni-201	0.0 ± 0.5	0.6	—	—
Hastelloy-N	2.3 ± 0.2	0.8	—	—
Incoloy-800H	28.6 ± 2.6	33.0	1.0	0.2 ± 0.2

Table 3 Salt Cr content measurements from 500 hrs, 850 °C, FLiNaK molten salt immersion tests. NAA was used to analyze salt from the graphite crucibles, whereas dissolution in aqua regia followed by ICP-OES was used for the Ni crucible salt analysis.

Alloy	Graphite crucible salt Cr content (ppm)	Ni crucible salt Cr content (ppm)	PyBN crucible salt Cr content (ppm)	800H crucible salt Cr content (ppm)
Blank salt	4.0 ± 0.5	<5.3	<5.3	4.0±0.5
Ni-201	3.6 ± 0.2	<4.9	—	—
Hastelloy-N	52.6 ± 2.7	<15.1	—	—
Incoloy-800H	371.9 ± 20.9	17.6	211.0	99.8 ± 5.1

100 cc/min argon purge was maintained above the carbon foam immersion cells to remove any residual moisture or impurities, but not otherwise introduce them into the stagnant gas space beneath the carbon foam. The argon purge gas contained <2 ppb O_2 and <20 ppb H_2O.

Results

Table 2 compares the weight loss of the alloys with varying Cr content in Ni, graphite, PyBN, and Incoloy-800H crucibles. The coupons in the graphite and Incoloy-800H crucibles were exposed in triplicate, whereas only single coupons were run in the Ni and PyBN crucibles. Ni-201 and Hastelloy-N coupons were not screened in the PyBN and Incoloy-800H crucibles. Because the Ni and PyBN crucible immersion tests used only single coupons, the variance in weight-loss between coupons exposed to identical conditions is unknown for those crucibles. The ratios of salt volume to salt-exposed coupon surface area, salt volume to salt-exposed crucible surface area, and salt-exposed coupon surface area to salt-exposed crucible surface area were kept constant for all tests. The Incoloy-800H crucible exposed surface area must be considered when considering the data in Table 2.

Immersion tests occurred over several years and institutions, and while effort was made to reproduce analyses as closely as possible, some differences remained, such as for salt analysis. ICP-OES (inductively coupled plasma optical emission spectrometry) proved unreliable for the tests performed at the UW due to inadequate dissolution procedures; dissolution issues were overcome by the analytical chemistry laboratory staff at SRNL (Savannah River National Laboratory) where ICP-OES was later utilized. Salt samples from the as-received (pre-alloy exposure) and immersion capsule tests were taken for analysis. The salts from the immersion tests with the first corrosion cell design, using graphite and Incoloy-800H crucibles, were analyzed using neutron activation analysis (NAA) at the University of Wisconsin Nuclear Reactor (UWNR). The salts from the immersion tests with the second corrosion cell design, using nickel and PyBN crucibles, were analyzed at SRNL by ICP-OES after dissolution in aqua regia. The Cr content of the salt in the graphite crucibles was much higher than that in the Ni crucibles, Table 3. The methodology of the NAA can be found in the thesis by Ludwig [18]. To a first approximation, the amount of Cr the Incoloy-800H crucible contributed in that immersion test is likely proportional to the ratio of the salt exposed crucible area (~260 cm^2) to the overall exposed alloy area (~284 cm^2). Therefore, the Incoloy-800H crucible likely contributed about 92% of the Cr, and 8% of the Cr detected likely came from the 3 Incoloy-800H samples.

Table 4 Salt Cr content measurements from 500 hrs, 850 °C, FLiNaK molten salt immersion tests in graphite crucibles but different salt sources. NAA was used for all analysis in Table 4.

Salt source	Blank salt Cr content (ppm)	800H coupon weight-loss (mg/cm^2)	800H exposure salt Cr content (ppm)
ECS	4.0 ± 0.5	28.6 ± 2.6	371.9 ± 20.9
INL	3.0 ± 0.5	20.7 ± 2.2	324.6 ± 16.7
UW	8.2 ± 0.9	24.7 ± 1.0	206.2 ± 5.1

The Cr levels in the salt for the graphite crucible exposures were correlated to alloy weight-loss and initial alloy Cr concentrations [8]. Comparing the salt analysis between crucible materials is complicated due to dispersed graphite suspensions in the salt that may have formed Cr carbides. If graphite is partially soluble or present in solution as a colloid, then the Cr FLiNaK solubility determined by NAA may appear to be larger than actual.

Table 4 presents post corrosion salt analysis obtained using NAA, from Incoloy-800H coupon immersion tests in graphite crucibles using FLiNaK salts from three sources. These salts were all fabricated from high purity ingredients, but underwent different processes to remove moisture and oxide impurities as described in the "Experimental" section. The ECS salt fabrication process was thought to have been the most thorough in removing impurities, followed by the INL process, with the UW process the least stringent. A spread in Cr concentrations was found in the exposed salt but similar weight-loss. It is hypothesized the differing corrosion rates or Cr concentrations of the salt could be from residual impurities from the salts or from the graphite test crucible. Graphite particulates dispersed in the salt may have led to some variation. In all three cases, the FLiNaK salts were fabricated in glassy carbon crucibles or graphite, and the immersion tests occurred in graphite crucibles described earlier. Although a cleaning procedure was used to remove fine graphite particulates from the graphite crucibles prior to the exposures, the effectiveness of this on removal of graphite particulates was not quantified.

Some of the salts had a darker appearance than others after the immersion tests. The salts from the graphite crucibles containing the Incoloy-800H were grey to black/brown in complexion, whereas the salt from the Ni-201 and Hastelloy-N immersions were bright white. Colloidal graphite and/or carbide particles likely discolored the salt. The primary Cr fluorides expected in the FLiNaK, CrF_2, and CrF_3 appear a shade of green, and dilute to a green color in solid salt. A green salt was observed in some FLiNaK immersion tests in performed Ni crucibles. Ozeryanaya et al. have described a process by which carbon or graphite material in molten NaCl may absorb ions and acquire a charge that in turn

stabilizes the colloidal particles of carbon [13]. It is hypothesized a similar process was responsible for the grey coloration of the salt and the variance in the salt Cr contents.

Characterization of Interaction of Fe–Cr and Ni–Cr Alloys With Graphite. The alloy coupons in the graphite immersion exposures were in intimate contact with graphite (fixturing rod and screws were made of graphite), during the alloy/molten salt exposure. Therefore, conditions that were necessary to facilitate galvanic corrosion were present. The alloys and graphite were likely far apart on the galvanic series (the author could find no complete galvanic series in FLiNaK, although EMF (electromotive force) tables for select elements exist). Assuming the molten salt dissolved any residual native oxide layers, the alloys and graphite were also in contact electrically and the molten salt served as an electrolyte. Because the molten salt is highly conductive, it is able to spread the corrosion over a large area of the less noble alloy, which would mask the otherwise telltale signs of galvanic corrosion (i.e., the corrosion at the junction of the alloy and the graphite did not appear worse than elsewhere on the alloy) [19]. The small area of the anodic coupon (nominally 8 cm^2 per coupon) paired with the large area of the cathodic graphite crucible (nominally 260 cm^2) promotes anodic dissolution [19].

A gray film was found on some of the graphite rods to which the coupons were attached and provided the first evidence of an interaction between graphite and the test alloy. The graphite components were then analyzed extensively using SEM (scanning electron microscopy), EDS (energy dispersive spectroscopy), XRD (X-ray diffraction), XPS (X-ray photoelectron spectroscopy), and RBS (Rutherford backscattering spectroscopy) techniques.

The film was present on the graphite fixturing rods from the Incoloy-800H exposures. This alloy had a high Cr content (~20%). There was no observed film on the Cr free Ni-201 and low Cr Hastelloy-N alloys.

The graphite rods were sectioned and a region immediately adjacent to the alloy coupons was examined. An EDS point scan (location designated as #1 in Fig. 5) of the Cr rich film present on the coupon rod from the Incoloy-800H crucible reported a measurement of 57.9 at. % carbon, 32.2% Cr, and 9.4% Fe, which results in about a 1:3 ratio of Fe:Cr (for Incoloy-800H the Fe:Cr ratio is about 2:1). EDS does not provide for a reliable, quantitative C determination due to C contamination from the environment.

Cross-sectional SEM and EDS X-ray maps show Cr and Fe present as a surface film on the Incoloy-800H coupon fixturing rod and that it did not penetrate deeply into it, Fig. 6. The thickness of the Cr rich layer varied between graphite rods for similar locations near the alloy coupons. The thickness of the films on the graphite rods therefore did not correlate with the weight-loss/area of the alloy test coupons.

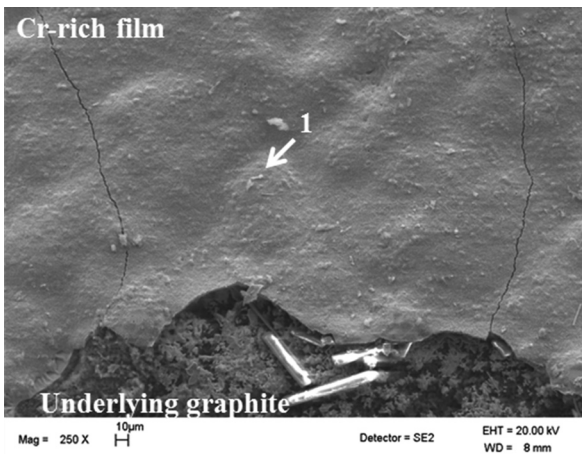

Fig. 5 SEM of Cr-rich film on graphite fixturing rod from Incoloy-800H containing crucible tests

Cr_7C_3 was detected with XRD, on the graphite fixturing rods from the Incoloy-800H molten salt exposures. The XRD data from the Incoloy-800H was consistent with Cr_7C_3 (Fig. 7), except for a peak shift of a few degrees, hypothesized to be from the 1:3 Fe:Cr atomic ratio.

XPS analysis of the Cr rich surface film from the Incoloy-800H coupon fixturing rod detected multiple C peaks (Fig. 8), with one at 282.7 eV associated with carbide formation [20]. While not shown, the XPS data from the Cr $2p_{3/2}$ and $2p_{1/2}$ peaks and from the Fe $2p_{3/2}$ peak also closely match XPS data from M. Detroye et al. for $[Fe, Cr]_7C_3$ [21].

Rutherford backscatter spectroscopy (RBS) was used to determine the concentration of Cr as a function of depth into the graphite crucible. EDS was not sensitive or precise enough to reliably detect Cr in the graphite crucible wall. The crucible that was used for the measurement was from immersion tests reported elsewhere and contained the alloy Hastelloy-X [7]. Hastelloy-X is similar to Incoloy-800H, but contains more Mo and Ni, and less Fe. Cr was detected and decreased with depth (Fig. 9), albeit at much lower concentrations (starting at near 5 at. % and decreasing to near zero within the first 1–2 μm). Small pore and particle sizes should result in decreased infiltration of graphite by the molten salt and Cr detection compared to graphite with larger pore and particle sizes. Comparing the Cr infiltration into the graphite crucible to that into the fixturing rod, it is evident the graphite crucible underwent the same reactions as the graphite fixturing rod; however, it is hypothesized that because the fixturing rod was in closer proximity to the coupons, more of the corrosion products deposited on the fixturing rods than the crucible walls.

Characterization of Interaction of Fe–Cr and Ni–Cr Alloys With Nickel. The alloy coupons in the Ni crucibles also met most of the preconditions for galvanic corrosion. Upon visual inspection crucibles and alloys appeared similar in condition as prior to exposure but with less polish, in contrast to the graphite crucibles. Due to the similar weight-loss to the coupons in the graphite crucible exposures, Table 2, it was hypothesized that the Ni crucibles were also acting as sinks for the Cr from the coupons (and perhaps Fe in the case of Incoloy-800H). A cross section of the Ni crucible from the Incoloy-800H molten salt exposure was mounted and examined under SEM/EDS, with an EDS line scan shown in Fig. 10. The EDS line scan shows that Cr had diffused into the Ni crucible to form a Ni–Cr alloy to a depth of ~70 μm. The depth of Cr diffusion into the Ni was similar to that seen for similar times and temperatures for Cr diffusion into Ni electroplated on Incoloy-800H, from the Incoloy-800H [4], but with a smaller maximum concentration of Cr.

Characterization of Interaction of Fe–Cr alloys With Similar Alloy and PyBN Crucibles. Due to the low weight-loss from the Incoloy-800H coupons in both the Incoloy-800H and PyBN crucibles, it was assumed the interaction between the coupons and both the crucible materials was negligible. Therefore, the crucibles and coupon fixturing materials were not examined in depth. In neither case, conditions for galvanic corrosion were met.

The PyBN crucible appeared nearly identical after the immersions as prior and was likely unwetted by the salt as evidenced by the salt falling out from the crucible by simple inversion. The salts from the Incoloy-800H crucible, similar to many of the salts from the graphite crucibles, occasionally required some encouragement to fall out of the crucibles.

Discussion

The weight-loss measured from the Incoloy-800H coupons in the Incoloy-800H capsule were 2 orders of magnitude less than

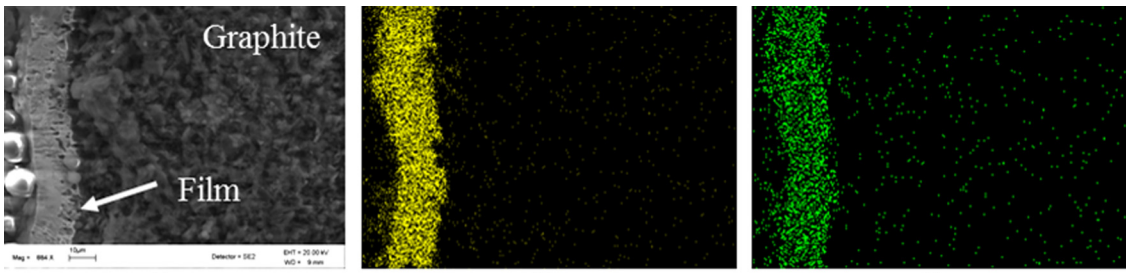

Fig. 6 SEM on graphite central fixturing rod from (*a*) Incoloy-800H corrosion experiments with a ~15 μm thick carbide layer. EDS X-ray mapping of elemental (*b*) Cr and (*c*) Fe, show the elements are concentrated on the surface and do not penetrate into the graphite.

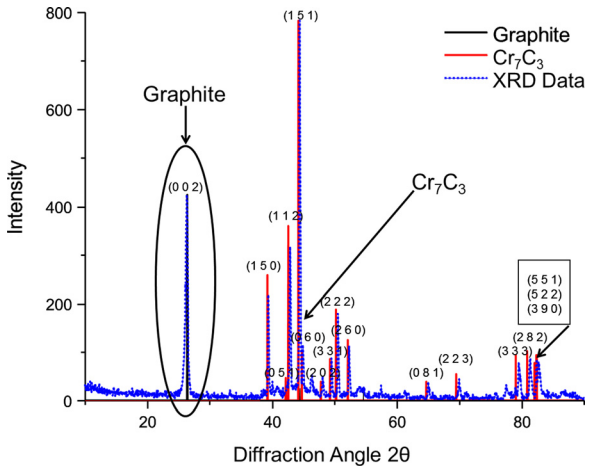

Fig. 7 XRD data showing identifying peaks for graphite and Cr_7C_3 from the Cr film present on the graphite fixturing rod from the Incoloy-800H containing crucible

those from the tests performed in the graphite crucible and slightly more than 1 order of magnitude less than in the PyBN crucible (Table 2). It is estimated the Incoloy-800H coupons contributed 8% of the Cr found in the salt from the Incoloy-800H immersion test based on exposed alloy area. This difference in weight-loss highlights the increase in corrosion of the alloy coupons due to graphite and Ni in the system promoting Cr de-alloying from the coupons by removing Cr from solution through the formation of Cr carbides or a Ni-Cr alloy.

Colloidal graphite particles may have been in solution and these could form carbides that can increase detected Cr contents in the

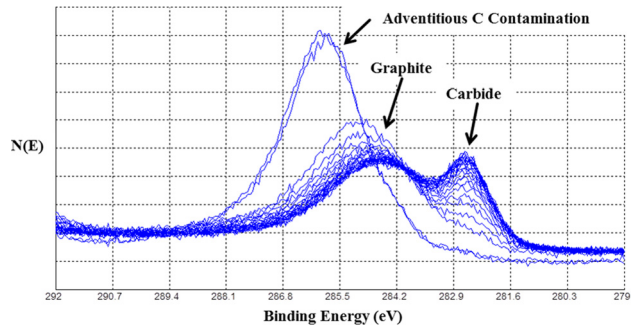

Fig. 8 XPS data from the Cr rich film found on the graphite rod that was used to fixture the Incoloy-800H coupons. The sample was progressively sputtered with Ar, followed by sampling of the electron binding energy, leading to a decreasing peak from C contamination and increasing peaks from the graphite rod and carbide.

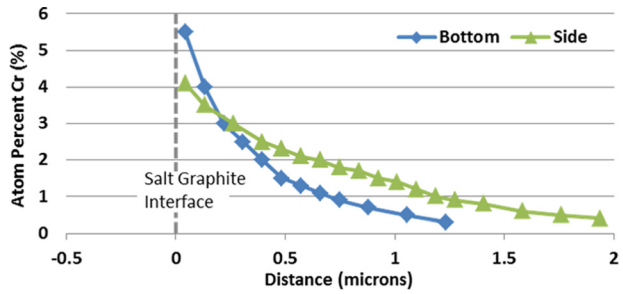

Fig. 9 RBS data from the graphite crucible's bottom and side that held Hastelloy-X coupons during the FLiNaK exposure test

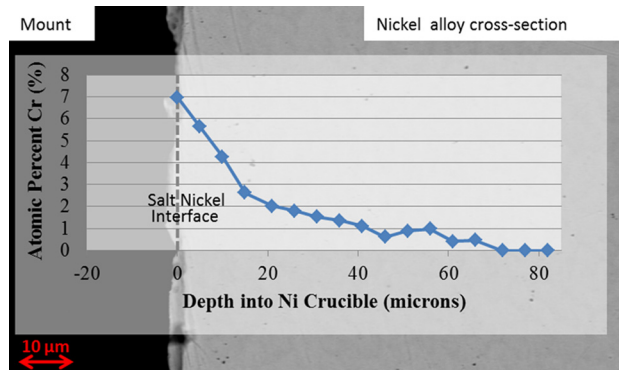

Fig. 10 EDS line scan taken from the Ni crucible containing a single Incoloy-800H coupon. The mounting material identified in the SEM image is located on the salt exposed side of the Ni crucible wall.

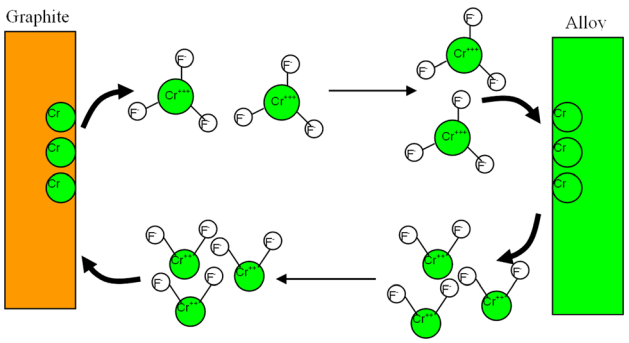

Fig. 11 Schematic of nonelectric transfer described by Ozeryanaya, as applied to the Fe–Ni–Cr/graphite/FLiNaK system

salt analysis (Table 3) performed on salts from the graphite crucible immersion tests. In the Ni crucibles, the crucible walls provided the only Cr sink without any graphite colloidal suspension in solution, and may have contributed to the lower measured values. When a Cr sink was not present the alloy–salt–crucible system attained a stable Cr concentration and the driving force for Cr dissolution from the alloy coupon dissipated.

Ozeryanaya [14] has summarized, for molten salt heat treatment baths, multiple corrosion processes which can result in the dealloying of elements that are susceptible to forming multiple oxidation states in molten salts and can alloy or react with the container material if alloy elemental constituents are more electropositive. Likewise, graphite may also take part in such processes if it is soluble in the salt and can form carbides with the elements with multiple oxidation states [14]. Pure FLiNaK is known to stabilize the CrF_3 and FeF_3, and the primary state of Cr metal in FLiNaK is CrF_3 [5].

Ozeryanaya [14] found that chemical attack, in chloride salt heat treatment baths, could occur by what he referred to as nonelectric transfer, although a more accurate description would be to call it activity gradient driven mass transfer. Electronegative metals (i.e., Cr) would dissolve into the salt with a low oxidation state (i.e., CrF_2) and would transfer to electropositive metals in the container alloys by a simultaneous oxidation (CrF_3) and reduction (Cr^0) provided the metals could form alloys with each other as exemplified in the following equation [14]:

$$3CrF_2 \leftrightarrow 2CrF_3 + Cr(Ni)_{alloy} \tag{1}$$

Graphite can also take part in nonelectric transfer provided that the metals can form carbides as exemplified in the following equation and Fig. 11 [14]:

$$3CrF_2 \leftrightarrow 2CrF_3 + Cr(C)_{carbide} \tag{2}$$

According to Ozeryanaya [14], nonelectric transfer increases with increasing: temperature, salt convection, and surface area of the electronegative metal. A more complete explanation may be that the Fermi levels are higher in the higher Cr alloys and lower in the lower Cr alloys, with the CrF_2 state favored in the proximity of the metal surface leading to Cr dissolution, likewise CrF_3 may be favored near the graphite or Ni interface, leading to the deposition of Cr.

The graphite capsules and fixturing rods appeared to accelerate the corrosion of the alloys by removing Cr from the solution in comparison to the PyBN crucibles. This leaves more F^- in the FLiNaK than otherwise would be, and therefore makes the salt more corrosive. Carbides formed in Hastelloy alloys principally in the grain boundaries have been found to be of the $[Cr, Fe]_{23}C_6$ variety [22], whereas those found on the graphite rods were identified as Cr_7C_3. The formation of Cr_7C_3 carbides from $Cr_{23}C_6$ carbides is thermodynamically favorable at 850 °C, because the change in Gibbs free energy of formation from the Cr carbide change from $Cr_{23}C_6$ to Cr_7C_3 is a negative change in Gibbs free energy

$$\begin{aligned} &7Cr_{23}C_6 + 27C \rightarrow 23Cr_7C_3 \\ &\Delta G_{FF} < 0 \end{aligned} \tag{3}$$

Cr transport to the graphite surface and subsequent carbide formation is now required. The reaction of CrF_3 with Cr is also thermodynamically favored leaving CrF_2 as product, i.e.,

$$\begin{aligned} &2CrF_3 + Cr \rightarrow 3CrF_2 \quad \text{and} \quad 46CrF_3 + Cr_{23}C_6 \rightarrow 69CrF_2 + 6C \\ &\Delta G < 0 \end{aligned} \tag{4}$$

But thermodynamically, the reactions occurring with the graphite are not thermodynamically favored without some other driving force, i.e.,

$$\begin{aligned} &3CrF_2 \rightarrow 2CrF_3 + Cr \quad \text{and} \quad 21CrF_2 + 3C \rightarrow 14CrF_3 + Cr_7C_3 \\ &\Delta G > 0 \end{aligned} \tag{5}$$

CrF_3 is stabilized in FLiNaK and has been found to be the dominant chemical state in solution [5]. It is speculated this tendency to form CrF_3 allows the reactions in Eq. (5) to occur in the basic molten FLiNaK salt.

For a thermodynamic equilibrium between the salt, crucible, and alloy to be established, the activity of the salt, crucible, and alloy must equalize. Thermodynamic equilibrium is an activity difference driven process and occurs by the removal of Cr from the alloy coupons into solution forming CrF_2 and from the removal of some of the CrF_2 from solution forming a Cr metal layer on the graphite (see Fig. 11). This requires the conversion of some of the CrF_2 to CrF_3 in solution because the graphite is noble and does not donate electrons for the reduction of CrF_2 to Cr. Once the Cr is deposited it then reacts with the graphite to form carbide ($\Delta G < 0$); the CrF_3 in solution then transports back to the surface of the coupon further allowing for dissolution of Cr from the alloy. The electron transfer at the alloy surface is driven by the potential difference between the crucible material and alloy. In the particular case of Cr forming a Cr layer on the graphite, the Cr metal layer proceeds to react with the graphite, forming Cr carbides. This changes the activity of the solid and allows for further depletion of the Cr in the salt causing corrosion of the alloy coupon to continue.

Recent research has found holding the salt sufficiently reducing by introduction of a reducing agent such as Mg, reduces the transfer of Cr through the above mechanism from a Cr rich alloy immersed in FLiNaK to a Ni crucible [23]. It is hypothesized reduction in Cr transfer occurs because the salt is held at a low redox state where the CrF_3 ion is not stable and free fluoride ions in solution are mostly tied up by Mg cations.

Conclusion

The graphite and Ni crucible presented Cr sinks that promoted the Cr dissolution process from the Cr bearing alloys by way of forming Cr-carbide and Cr alloy phases on the surface of the graphite and Ni crucible components, respectively. SEM evaluation of the Incoloy-800H coupons from the crucibles and salt analysis showed that the mechanism of corrosion for the differing crucible exposures was largely identical, although differed in magnitude.

The heightened Cr dissolution in FLiNaK from high Cr alloys in graphite and Ni crucibles may have occurred due to interactions of $Cr^{2+/3+}$ states with the alloy, salt, and graphite/Ni. Cr dealloys from the coupons and forms Cr fluorides in the salt; the Cr in the salt then deposits on the graphite/Ni from solution. This process continues until a thermodynamic equilibrium is established between the alloy, salt, and crucible. From NAA, it was seen that the Cr content of the salt from a 500 hrs at 850 °C exposure for Incoloy-800H in an Incoloy-800H crucible in FLiNaK was ~100 ppm, whereas it was ~4× higher for the same alloy in a graphite capsule. A Cr_7C_3 film was identified on the graphite rod used to hold the Incoloy-800H coupons and Ni-Cr alloying was observed in the Ni crucible. Furthermore, the salt from several corrosion tests had a grayish appearance pointing toward colloidal graphite and or carbide suspensions in the salt, but the salt only had a greenish appearance in the most aggressive Ni crucible exposures with the most observed coupon weight-loss. Formation of carbides for the graphite crucibles or Cr–Ni alloy for the Ni crucibles increased chemical activity.

It is recommended based on this work that PyBN be used if a noninteracting crucible is desired in a fluoride salt melt. Alternatively, it has been found in recent research that use of reducing agents can suppress the mass transfer reaction of Cr due to activity gradients. If research is being undertaken to simulate mass transfer reactions, then Ni or graphite crucibles may be acceptable, so

long as differences in the transport mechanisms are understood. However, Ni crucibles are recommended for mass transfer studies because it is difficult to eliminate carbon contaminants in graphite crucibles.

Acknowledgment

Portions of this work were supported by the DOE-EERE SunShot Initiative and DOE-NE NERI and NEUP programs, under DOE Grants No. Garcia-Diaz_A, DOE-FC07-05ID14675 and DOE_FC07_07ID14826. Portions of this research utilized NSF-supported shared facilities at the UW. The portions of the work performed under DOE Grants No. Garcia-Diaz_A were performed by DOE contractors working for Savannah River Nuclear Solutions at Savannah River National Laboratory.

References

[1] Misra, A., and Whittenberger, J., 1987, "Fluoride Salts and Container Materials for Thermal Energy Storage Applications in the Temperature Range 973 to 1400 K," NASA Lewis Research Center, Cleveland, OH, Technical Memorandum No. 89913.

[2] Forsberg, C., Peterson, P., and Zhao, H., 2007, "High-Temperature Liquid-Fluoride-Salt Closed-Brayton-Cycle Solar Power Towers," ASME J. Sol. Energy Eng., **129**(2), pp. 141–146.

[3] Greene, S., Holcomb, D., Gehin, J., Carbajo, J., Cisneros, A., Corwin, W., Ilas, D., Wilson, D., Varma, V., Bradley, E., and Yoder, G., 2010, "SMAHTR—A Concept for a Small, Modular Advanced High Temperature Reactor," Fifth International Conference on High Temperature Reactor Technology (HTR 2010), Prague, Czech Republic, Oct. 18–20, Paper No. 205.

[4] Schmidt, J., Scheiffele, M., Crippa, M., Peterson, P., Urquiza, E., Sridharan, K., Chen, Y., Olson, L., Anderson, M., and Allen, T., 2011, "Design, Fabrication and Testing of Ceramic Plate Type Heat Exchangers with Integrated Flow Channel Design," Int. J. Appl. Ceram. Technol., **8**(5), pp. 1073–1086.

[5] Williams, D., Toth, L., and Clarno, K., 2006, "Assessment of Candidate Molten Salt Coolants for the Advanced High-Temperature Reactor (AHTR)," Oak Ridge National Laboratory, Oak Ridge, TN, Report No. ORNL/TM-2006/1.

[6] Olson, L., Ambrosek, J., Sridharan, K., Anderson, M., and Allen, T., 2009, "Materials Corrosion in Molten LiF–NaF–KF Salt," J. Fluorine Chem., **130**(1), pp. 67–73.

[7] Olson, L., 2009, "Materials Corrosion in Molten LiF–NaF–KF Eutectic Salt," *Engineering Physics2009*, University of Wisconsin-Madison, Madison, WI.

[8] Olson, L., Sridharan, K., Anderson, M., and Allen, T., 2010, "Intergranular Corrosion of High Temperature Alloys in Molten Fluoride Salts," Mater. High Temp., **27**(2), pp. 145–149.

[9] DeVan, J. H., 1969, "Effect of Alloying Additions on Corrosion Behavior of Nickel–Molybdenum Alloys in Fused Fluoride Mixtures," Vol. I, Oak Ridge National Laboratory, Oak Ridge, TN, Technical Document No. ORNl-TM-2021.

[10] Prasad, S., 2000, "The Principle Problems of Aluminum Electrowinning: An Update," Br. J. Chem. Eng., **17**(2), pp. 211–218.

[11] Godding, A., and DeAntonio, D., 1991, "Liquid Carburizing and Cyaniding," *ASM Handbook: Heat Treating*, ASM International, Materials Park, OH, pp. 329–347, 793–814.

[12] Becherer, B., 1991, "Processes and Furnace Equipment for Heat Treating of Tool Steels," *ASM Handbook: Heat Treating*, ASM International, Materials Park, OH, pp. 726–733.

[13] Ozeryanaya, I., Zalanzinski, G., Smirnov, M., Finkel'shtein, S., and Shamanova, N., 1975, "Corrosion of Molybdenum in Molten Sodium Chloride in the Presence of Carbon," Zashch. Met., **11**(1), pp. 66–68.

[14] Ozeryanaya, I., 1985, "Corrosion of Metals by Molten Salts in Heat-Treatment Processes," Metal Sci. Heat Treat., **27**(3), pp. 184–188.

[15] Williams, D., Wilson, D., Keiser, J., Toth, L., and Caja, J., 2003, "Research on Molten Fluorides as High Temperature Heat Transfer Agents," Global 2003, Session 2A: Coolant/Material Interactions in Advanced Reactor Systems, Embedded Topical Within 2003 American Nuclear Society Winter Meeting, New Orleans, LA, Nov. 16–20.

[16] Poco, 2013, "AXZ-5Q," Poco Graphite Inc., Decatur, TX, accessed Dec. 17, 2013, http://www.poco.com/tabid/92/Default.aspx

[17] Sheppard, R., Mathes, D., and Bray, D., 2001, "Poco Graphite, Inc. Properties and Characteristics of Graphite for Industrial Applications," Poco Graphite Inc., Decatur, TX, Report No. 60038.

[18] Ludwig, D., 2008, "Analysis Techniques for Corrosion Product Detection in Molten Salts: High Temperature Electrochemistry and Neutron Activation Analysis," *Engineering Physics 2008*, University of Wisconsin-Madison, Madison, WI.

[19] Jones, D. A., 1996, *Principles and Prevention of Corrosion*, 2nd ed., Prentice Hall, Upper Saddle River, NJ.

[20] Tabet, N., Allam, I., and Yin, R., 2003, "X-Ray Photoelectron Spectroscopy Investigation of the Carburization of 310 Stainless Steel," Appl. Surf. Sci., **220**(1–4), pp. 259–272.

[21] Detroye, M., Reniers, F., Buess-Herman, C., and Vereecken, J., 1999, "AES-XPS Study of Chromium Carbides and Chromium Iron Carbides," Appl. Surf. Sci., **144–145**, pp. 78–82.

[22] Streicher, M., 1976, "Effect of Composition and Structure on Crevice, Intergranular, and Stress Corrosion of Some Wrought Ni–Cr–Mo Alloys," Corrosion-NACE, **32**(3), pp. 79–93.

[23] Olson, L., Fuentes, R., Martinez-Rodriguez, M., Garcia-Diaz, B., and Gray, J., 2014, "Reducing Agent Effects on Haynes-230 in Molten Halide Salts," ANS Annual Meeting, Reno, NV, June 15–19, pp. 859–862.